CHEMBIOCHEM

DOI: 10.1002/cbic.201100161

Synthesis and Structural Characterization of 2′-Fluoro-α-L-RNA-Modified Oligonucleotides

Troels Bundgaard Jensen, Anna Pasternak, Andreas Stahl Madsen, Michael Petersen, and Jesper Wengel*[a]

We describe the synthesis and binding properties of oligonucleotides that contain one or more 2′-fluoro-α-L-RNA thymine monomer(s). Incorporation of 2′-fluoro-α-L-RNA thymine into oligodeoxynucleotides decreased thermal binding stability slightly upon hybridization with complementary DNA and RNA with the smallest destabilization towards RNA. Thermodynamic data show that the duplex formation with 2′-fluoro-α-L-RNA nucleotides is enthalpically disfavored but entropically favored. 2′-Fluoro-α-L-RNA nucleotides exhibit very good base pairing specificity following Watson–Crick rules. The 2′-fluoro-α-L-RNA monomer was designed as a monocyclic mimic of the bicyclic α-L-LNA, and molecular modeling showed that this indeed is the case as the 2′-fluoro monomer adopts a C3′-*endo*/C2′-*exo* sugar pucker. Molecular modeling of modified duplexes show that the 2′-fluoro-α-L-RNA nucleotides partake in Watson–Crick base pairing and nucleobase stacking when incorporated in duplexes while the unnatural α-L-*ribo* configured geometry of the sugar is absorbed by changes in the sugar–phosphate backbone torsion angles. The duplex behavior of our new nucleotide follows that of α-L-LNA, by and large.

Introduction

Chemically modified oligonucleotides (ONs) are broadly applied within the field of nucleic acid chemical biology to improve properties, like resistance against enzymatic degradation and binding affinity toward DNA and RNA.[1–3] Modification at the 2′-position of the furanose ring has been a preferred strategy towards increasing the RNA-binding affinity and nucleolytic resistance. Introducing a 2′-fluorine substituent instead of the 2′-hydroxy group has been intensively studied as fluorine and the hydroxy group are similar in size while their electronegativity and hydrogen bond behavior are different.[4–6] Introduction of 2′-deoxy-2′-fluoro-β-D-ribonucleic acid (2′-F-RNA) monomers[7,8] into DNA ONs induces increased thermal stability of duplexes formed with RNA complements; this is explained by the fact that 2′-F-RNA is an RNA mimic and its furanose ring adopts a C3′-*endo* pucker.[9,10] The use of 2′-F-RNA within antisense mediated gene silencing has been limited by the fact that 2′-F-RNA-modified antisense ONs, except the so-called gapmers, are unable to induce RNase H-mediated cleavage of an RNA target.[4,11] Inversion of the stereochemistry at the C2′-position of 2′-F-RNA results in 2′-deoxy-2′-fluoro-β-D-arabinonucleic acid (2′-F-ANA; Figure 1).[6,7,12,13] Introduction of 2′-F-ANA monomers into DNA ONs likewise induces increased thermal stability of duplexes formed with DNA and RNA complements.[14] 2′-F-ANA is a DNA mimic as the furanose moiety adopts an O4′-*endo* pucker;[13] this has stimulated its use in the antisense field as 2′-F-ANA-modified antisense ONs induce RNase H-mediated cleavage of a complementary RNA strand, although cleavage rates are generally lower than with unmodified DNA ONs.[15,16]

Previously we have reported ONs containing the DNA-mimicking monomers α-L-LNA[17,18] and α-L-RNA[19,20] (Figure 1). An α-L-LNA (α-L-*ribo*-configured locked nucleic acid) monomer has the same constitution as an LNA monomer with a 2′-*O*-4′-*C*-methylene-linked furanose ring but inversed configuration at three of its stereocenters. ONs containing α-L-LNA show appealing hybridization properties towards RNA comple-

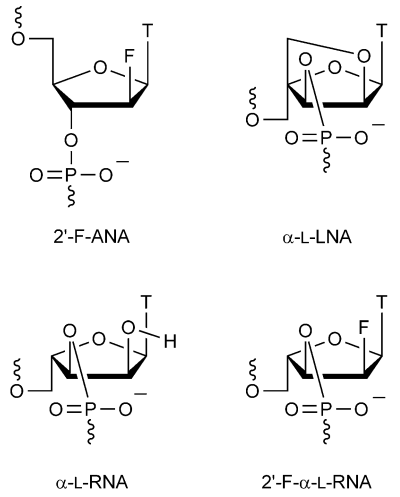

Figure 1. Selected DNA-mimicking nucleotides. In Tables 1 and 2, the notations $^{\alpha L}\mathbf{T}^{L}$ (α-L-LNA), $^{\alpha L}\mathbf{T}$ (α-L-RNA) and **X** (2′-F-α-L-RNA) are used for the three different α-L-*ribo* configured monomers; T: thymin-1-yl.

[a] *Dr. T. Bundgaard Jensen, Dr. A. Pasternak, Dr. A. Stahl Madsen, Dr. M. Petersen, Prof. J. Wengel*
Nucleic Acid Center, Department of Physics and Chemistry
University of Southern Denmark, Campusvej 55
5230 Odense M (Denmark)
E-mail: jwe@ifk.sdu.dk

Supporting information for this article is available on the WWW under http://dx.doi.org/10.1002/cbic.201100161.

ments.[21,22] The furanose conformation of an α-L-LNA monomer is *N*-type (C3′-*endo*, ^{3}E) but it is a DNA mimic as a consequence of the unnatural L configuration.[23] NMR spectroscopic studies as well as molecular modeling simulations of partially and fully modified α-L-LNA:RNA duplexes have shown very similar overall duplex geometry to the corresponding unmodified DNA:RNA duplex, although some local rearrangements of the phosphate backbone were observed to accommodate the unnatural α-L-LNA nucleotides.[23–25] Despite the DNA-mimicking nature of α-L-LNA, antisense ONs containing such monomers induce only limited RNase H-mediated cleavage of complementary RNA.[24] RNase H recognizes a DNA:RNA duplex by interacting within the minor groove, and an NMR structure of a duplex between an α-L-LNA containing DNA ON with the RNA complement has revealed that the phosphate groups adjoining α-L-LNA nucleotides are rotated into the minor groove, which likely results in suboptimal geometries for RNA cleavage.[24] α-L-RNA monomers[19,20] have the same constitution as α-L-LNA monomers but lack the methylene group between the O2′ and C4′ atoms. Thus, being more structurally flexible than α-L-LNA, it was not surprising to observe that incorporation of α-L-RNA monomers into ONs induces decreased thermal binding affinity toward DNA and RNA complements, although with a preferential binding towards complementary RNA as also observed for α-L-LNA.[19,20] Interestingly, it was demonstrated that DNA ONs containing a single α-L-RNA monomer retain the ability to elicit RNase H activity.[19]

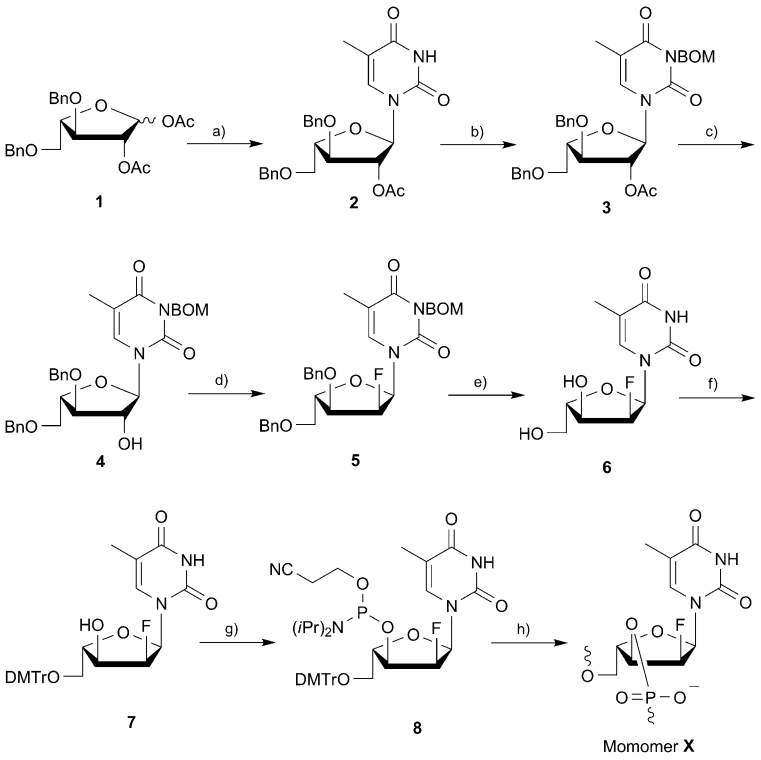

Scheme 1. Synthesis of 2′-F-α-L-RNA phosphoramidite derivative **8**. Reagents and conditions (yield): a) BSA, TMSOTf, thymine, MeCN, 80 °C (92%); b) BOMCl, DBU, DMF, room temperature (94%); c) sat. methanolic ammonia, CH_2Cl_2, room temperature (99%); d) pyridine, bis(methoxyethyl)aminosulfur trifluoride, toluene, room temperature (50%); e) i: BCl_3, CH_2Cl_2, −78 °C; ii: H_2O, room temperature (77%); f) DMTrCl, pyridine, room temperature (88%); g) diisopropylammonium tetrazolide, bis(*N*,*N*-diisopropylamino)-2-cyanoethoxyphosphine, CH_2Cl_2, room temperature (94%); h) automated ON synthesis.

Inspired by the excellent RNA targeting potential of α-L-LNA-modified ONs and their interesting behavior as outlined above, we have now synthesized the 2′-F-α-L-RNA monomer (Figure 1). This allows us to compare the effect of a monocyclic α-L-configured sugar with the bicyclic α-L-LNA sugar and to compare the effect of the 2′-fluorine substituent with a 2′-hydroxy group as found in α-L-RNA. To this end we have evaluated the thermostability of 2′-F-α-L-RNA-modified duplexes, derived thermodynamic data for duplex formation and performed molecular modeling at both the monomer and duplex level.

Results and Discussion

Synthesis

Phosphoramidite building block **8**, suitable for incorporation of 2′-F-α-L-RNA monomer **X** into ONs, was synthesized (Scheme 1). The known coupling sugar **1** was synthesized by using a previously published procedure,[26] and subsequent standard Vorbrüggen glycosylation afforded intermediate **2**. Fluorination was envisioned to be performed in a two-step inversion reaction, and as pyrimidine nucleosides are known to form 2,2′-anhydro intermediates, it was necessary to protect the N3-position of the thymine unit. This was achieved by introducing a BOM (benzyloxymethyl) group to give nucleoside **3**. Cleavage of the O2′ ester was carried out by using saturated methanolic ammonia to afford nucleoside **4**, which was then treated with deoxofluor [bis(2-methoxyethyl)aminosulfur trifluoride] to give the fluorinated nucleoside **5** with the C2′ stereocenter inverted. Removal of the protection groups was achieved by using BCl_3 to give nucleoside **6**, which was selectively protected at the O5′-position by treatment with DMTrCl (4,4′-dimethoxytritylchloride). The thus obtained nucleoside **7** was eventually subjected to standard phosphitylation to afford the desired phosphoramidite **8** in 27% overall yield calculated from starting sugar **1**. The configuration of compound **6** was verified by a NOESY experiment (Figure S11 in the Supporting Information). Cross-correlations were observed between H1′ and H2′ as well as H2′ and H3′ showing close proximity of these atoms. As the stereoconfiguration at the 3′-position was retained during the synthesis, this experiment verifies the α-L-*ribo* configuration of compounds **6**–**8** and monomer **X**.

Synthesis of ONs containing monomer **X** was performed on the 0.2 μmol scale with an automated DNA synthesizer. Standard cycle protocols were used for unmodified phosphoramidites (2 min coupling time, 1*H*-tetrazole as activator) whereas extended coupling time (15 min) was used for phosphoramidite **8**, resulting in stepwise coupling yields above 95%. All synthesized ONs were, if necessary, purified by RP-HPLC, and

their composition and purity (> 80%) were confirmed by MALDI-MS (Table S3 in the Supporting Information) and ion-exchange HPLC, respectively.

Table 1. Thermal denaturation temperatures (T_m values) of matched and singly mismatched duplexes.[a]

			T_m [°C]							
			DNA: 3′-CACT**B**TACG				RNA: 3′-CACU**B**UACG			
ON	Sequence	B=	A	T	G	C	A	U	G	C
ON1	5′-GTGATATGC		28.5	13.5	20.0	13.5	26.5	13.5	22.0	< 5
ON2	5′-GTGA**X**ATGC		26.0	< 5	14.5	< 5	25.5	< 5	18.0	11.5

[a] The T_m values were measured as the maximum of the first derivatives of the melting curves (A_{260} vs. temperature) recorded in a medium salt buffer (100 mM NaCl, 0.1 mM EDTA, 10 mM NaH_2PO_4, 5 mM Na_2HPO_4, pH 7.0) by using 1.0 μM of each of the two complementary strands. The T_m values are averages of at least two measurements.

Table 2. Thermal denaturation temperatures (T_m values)[a] and thermodynamic data.[b]

		T_m [°C]		$-\Delta G^\circ_{37}$ [kcal mol^{-1}]	
ON	Sequence	DNA	RNA	DNA	RNA
ON1	5′-GTGATATGC	28.5 30[c]	26.5 28[c]	6.82 ± 0.16	6.29 ± 0.15
ON2	5′-GTGA**X**ATGC	26.0	25.5	6.31 ± 0.06	6.22 ± 0.14
ON3	5′-GTGA($^{\alpha L}$**T**)ATGC	26[c]	28[c]	–	–
ON4	5′-GTGA($^{\alpha L}$**T**^{L})ATGC	34.5	34.0	8.14 ± 0.09	8.30 ± 0.14
ON5	5′-G**X**GA**X**A**X**GC	< 5	14.5	–	–
ON6	5′-G($^{\alpha L}$**T**)GA($^{\alpha L}$**T**)A($^{\alpha L}$**T**)GC	< 5[c]	12[c]	–	–
ON7	5′-T_{10}	17.5 20[c]	13.5 19[c]	–	–
ON8	5′-$\mathbf{X}_9$T	< 5	< 5	–	–
ON9	5′-($^{\alpha L}$**T**)$_9$T	< 5[c]	< 5[c]	–	–
ON10	5′-($^{\alpha L}$**T**^{L})$_9$T	63[c]	66[c]	–	–
ON11	5′-[(**X**)($^{\alpha L}$**T**^{L})]$_4$(**X**)T	< 5	< 5	–	–
ON12	5′-[($^{\alpha L}$**T**)($^{\alpha L}$**T**^{L})]$_4$($^{\alpha L}$**T**)T	< 5[c]	27[c]	–	–

[a] The T_m values were measured as the maximum of the first derivatives of the melting curves (A_{260} vs temperature) recorded in a medium salt buffer (100 mM NaCl, 0.1 mM EDTA, 10 mM NaH_2PO_4, 5 mM Na_2HPO_4, pH 7.0) by using 1.0 μM of each of the two complementary strands. The T_m values are averages of at least two measurements. [b] For the thermodynamic data of helix formation, see Table S5 in the Supporting Information. [c] From ref. [19]. $^{\alpha L}$**T**^{L}: α-L-LNA; $^{\alpha L}$**T**: α-L-RNA; **X**: 2′-F-α-L-RNA.

Thermal denaturation and thermodynamic studies

Initially, the effect of a single incorporation of monomer **X** on duplex stability was evaluated by thermal denaturation studies by using a medium salt buffer (Table 1). A slight decrease in thermostability was observed against both DNA and RNA complementary strands with monomer **X** being tolerated better in the RNA context. Furthermore, mismatch discrimination studies were carried out to investigate if monomer **X** participates in base pairing with the opposing nucleotide (Table 1). Improved mismatch discrimination relative to the unmodified oligonucleotide (**ON1**) was observed against both DNA and RNA targets, which shows that monomer **X** partakes in Watson–Crick base pairing.

In Table 2 is included a direct comparison of the effect on thermal denaturation temperature of monomers **X** and α-L-RNA (**ON2**, **ON3**, **ON5** and **ON6**). It is clear that substitution of the 2′-hydroxy group of an α-L-RNA monomer with a 2′-fluoro substituent has no major influence on the thermal stability of the resulting duplexes.

We next determined the thermodynamic parameters for the 9-mer **ON1** and its variants modified with either **X** (**ON2**) or α-L-LNA (**ON4**) hybridized with DNA and RNA complements (Table 2 and Table S5 in the Supporting Information). It should be noted that melting temperatures for the duplexes follow the trend of Table 1, and in accordance with the literature a single α-L-LNA modification yields a significant elevation in melting temperature. Introduction of monomer **X** into the DNA:DNA duplex decreased the thermodynamic stability by 0.51 kcal mol^{-1} relative to the unmodified duplex, whereas an α-L-LNA monomer made the duplex more stable by 1.32 kcal mol^{-1}. When hybridized with DNA, the **X**-modified **ON2** resulted in a less enthalpically favored and less entropically disfavored duplex relative to the unmodified all-DNA duplex (Table S5 in the Supporting Information). A similar trend seems to be observed for **ON4** hybridized with DNA, however, here the limits of errors for ΔH° and ΔS° values restrict further conclusions to be drawn. The less unfavorable entropy term of the **X**-modified duplex formation might be due to the constrained sugar moiety but changes in solvation will also contribute to this term. The less favorable enthalpic term is difficult to explain readily in terms of structure as our modeling of **X**-modified DNA duplexes (see below) show no large structural differences between modified and unmodified duplexes. The change in enthalpy might be due to an unfavourable backbone geometry imposed by the α-L-configured sugar or small changes in stacking interactions.

The thermodynamic picture is slightly different when the **X** and α-L-LNA-modified oligonucleotides are hybridized with RNA. The presence of monomer **X** within a DNA:RNA heteroduplex did not induce any significant change of Gibbs free energy, whereas introduction of α-L-LNA within the DNA strand of the DNA:RNA heteroduplex considerably improved thermodynamic stability. Our modeling in this study and previous NMR structures show that the α-L-LNA nucleobases appear to partake in efficient Watson–Crick pairing and stacking without much change from unmodified duplexes. However, a quantitative energetic description would require high level quantum mechanical calculations on base stacking and

backbone geometry, which is outside the scope of the present study.

Finally, different combinations of the monomers were evaluated in a homothymine 10-mer context. As reported earlier, the almost fully modified α-L-LNA (**ON10**) displayed high thermostability towards both DNA and RNA complements relative to the unmodified reference (**ON7**).[19] In contrast, the corresponding ONs containing 2′-F-α-L-RNA (**ON8**) or α-L-RNA (**ON9**) monomers melted below 5 °C when hybridized with DNA and RNA complements under medium salt conditions, whereas duplexes of low stability were observed for **ON8** hybridized with DNA and RNA complements at high salt conditions, again with preferential binding towards RNA (Table S4 in the Supporting Information). **ON12**, containing alternating α-L-RNA and α-L-LNA monomers displayed efficient hybridization with RNA but no melting was observed with its DNA complement. No melting was observed for the corresponding **ON11**, which contains 2′-F-α-L-RNA monomers, **X**, instead of α-L-RNA monomers, not even with RNA or at high salt concentration (Table S4 in the Supporting Information).

Modeling of monomers

In an attempt to explain the results from the thermal denaturation and thermodynamic studies described above, we analyzed the sugar conformations of the **X** monomer using quantum mechanical calculations and compared it with the sugar conformations of α-L-RNA and α-L-LNA. Each of the three α-L-configured nucleosides have a deep energy minimum for conformations with a pseudorotational angle close to zero with α-L-LNA showing the most shallow energy curve (data not shown). Thus, all these nucleosides are constrained in the *N*-range of the pseudorotation cycle. We also scanned the rotation profile of the glycosidic angle χ for the three α-L-configured nucleosides and again the results were similar with a global minimum near $\chi = -150^{\circ}$ and a local high-energy minimum, $\Delta E \geq 5$ kcal mol^{-1}, near $\chi = 50^{\circ}$. Having established conformational similarities at the monomeric level we proceeded towards evaluating the structural characteristics at the duplex level using CD for overall conformational features and molecular modeling for detailed atomic information (vide infra).

Circular dichroism curves

CD spectroscopy was employed to obtain insight into the helical structure of the 2′-F-α-L-RNA-modified duplexes (Figure 2). **ON2** hybridized with complementary DNA and RNA gave spectra displaying the characteristic features of B-type and intermediate A:B-type duplexes, respectively.[27] The unmodified duplexes gave virtually identical spectra; this indicates that the 2′-F-α-L-RNA monomer does not perturb the global helical structures despite its unnatural sugar configuration.

Molecular modeling of duplexes

To obtain an atomic insight into the features of the α-L-modified duplexes, we performed molecular dynamic simulations

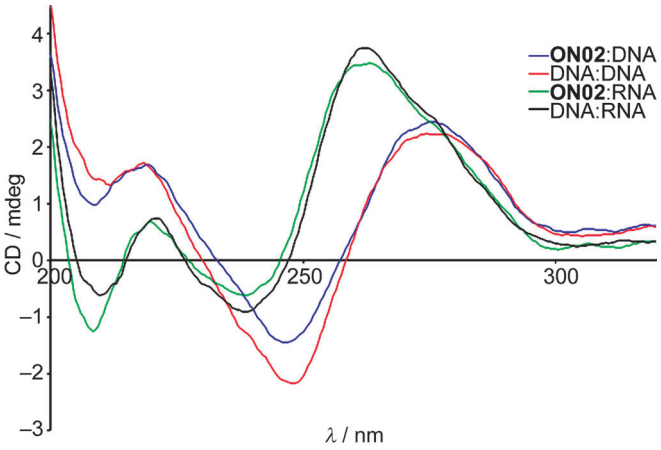

Figure 2. CD spectra of duplexes of **ON2** hybridized with complementary DNA and RNA as well as of unmodified reference duplexes.

with **ON2** hybridized with DNA and RNA complements and with ONs containing either an α-L-RNA or α-L-LNA monomer. We used starting structures with standard B- and A-type duplex geometries for the simulations of dsDNA duplexes and DNA:RNA hybrids, respectively, as justified by CD spectroscopy. All duplexes were subjected to molecular dynamics followed by energy minimization of snapshots by using the AMBER force field[28,29] and the GB/SA solvent model[30] as implemented in MacroModel V.9.1.[31]

In agreement with the thermal denaturation experiments, all simulations showed that the modified nucleotides are accommodated in the duplexes and partake in Watson–Crick base pairing and nucleobase stacking. As expected from the CD measurements, the global geometry of the modified duplexes is close to the geometries obtained in the simulations of the unmodified duplexes. The local geometry is, however, changed as a consequence of the configuration of the sugars (Figure 3).

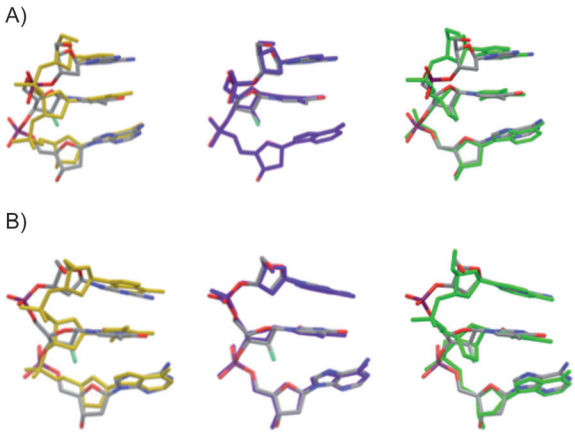

Figure 3. A) Duplexes formed with the DNA complement. Overlays of a three-nucleotide excerpt containing 2′-F-α-L-RNA monomer **X** (multicolored) with DNA (yellow), α-L-RNA (purple) and α-L-LNA (green). B) Corresponding duplexes formed with the RNA complement. Overlays of a three-nucleotide excerpt containing 2′-F-α-L-RNA monomer **X** (multicolored) with DNA (yellow), α-L-RNA (purple) and α-L-LNA (green). For clarity, all hydrogen atoms and sodium ions are omitted.

There is limited change in the positions of the nucleobases of the modified nucleotides. This demonstrates that base pairing and stacking govern the position of the nucleobases while the malleable sugar–phosphate backbone is left to alter its geometry so as to present the bases in optimum positions for base pairing and stacking. This is similar to what has been observed in NMR structures of α-L-LNA-modified duplexes.[24,25] First of all, the glycosidic angles of the modified nucleotides change from approximately −140° in the unmodified duplexes to values near −180° in the modified nucleotides with smaller changes observed for 2′-F-α-L-RNA and α-L-RNA monomers in a dsDNA context. This trend follows the results obtained by modeling at nucleoside level albeit the exact values differ.

The sugar puckers of the L nucleosides are of the *N* type. The 2′-F-α-L-RNA and α-L-RNA monomers show identical puckering (C3′-*endo*/C2′-*exo*) whereas the α-L-LNA monomer display a C3′-*endo* puckering as reported earlier.[23] Again this follows the trend of our quantum mechanical nucleoside calculations described above, and validates the simulation as carried out in the MacroModel environment.

As seen in Figure 3, the conformation of the sugar–phosphate backbone is dramatically altered in the modified duplexes as compared to the unmodified duplexes. Common changes are in the γ-, δ- and ζ-torsion angles from (*gauche*+, *gauche*+ and *gauche*−) to (*trans*, *gauche*− and *gauche*+), respectively. Similar changes were observed in NMR structures of α-L-LNA-modified duplexes.[24,25] Moreover, changes in the α- and β-torsion angles were observed for the 2′-F-α-L-RNA nucleotide, monomer **X** and the α-L-RNA monomer when hybridized with DNA. Furthermore, changes in the backbone torsion angles of the 3′-flanking nucleotides were also observed. In the unmodified duplexes, the α- and γ-torsion angles adopt a (*gauche*−, *gauche*+) conformation, which is the conformation with the lowest energy and consequently the most populated.[32] However, in the duplexes containing the three α-L-*ribo* configured monomers, the α- and γ-torsion angles adopt a (*gauche*+, *trans*) conformation. Such changes have previously been observed for α-L-LNA-modified duplexes.[24,25]

To summarize, all L nucleotides incorporated into ONs displayed a pronounced *N*-type sugar conformation as well as an *anti* conformation of the glycosidic torsion angle. Furthermore, rearrangements of the phosphate backbone were observed to accommodate the unnatural L nucleotides, as well as rearrangements of the backbone torsion angles the 3′-flanking nucleotide.

For the corresponding 2′-F-ANA derivative, the presence of a weak interaction between the 2′-F substituent and a nucleobase has been reported to be one of the causes of stabilization of the duplexes observed by incorporation of 2′-F-ANA nucleotides.[6] To what extent a similar interaction takes place with the 2′-F-α-L-RNA nucleotide **X** is unclear but the similar duplex stabilities obtained for monomer **X** and the corresponding α-L-RNA nucleotide (Table 2) suggest such an interaction to be very weak at best.

Conclusions

We have synthesized the 2′-fluoro-α-L-ribofuranose thymine phosphoramidite building block **8** in 27% overall yield and used it for incorporation of the 2′-F-α-L-RNA monomer **X** into oligonucleotides. A single incorporation of **X** is well tolerated in duplexes, although comparison with unmodified reference duplexes revealed a slight decrease in stability when hybridized with complementary DNA and RNA. Substitution of the 2-hydroxy group of an α-L-RNA monomer to a 2′-fluorine substituent did not induce a stabilizing effect in a duplex context. Three incorporations of monomer **X** induce a large decrease in duplex stability, with a preferential binding towards an RNA complementary strand. Molecular modeling showed that the conformation of the furanose ring of monomer **X** and α-L-RNA thymine adopt a C3′-*endo*/C2′-*exo* pucker whereas the α-L-LNA thymine adopts a C3′-*endo* pucker. Moreover, in order to compensate for the unusual configuration of monomer **X**, the phosphate backbone must undergo structural changes. In summary, the novel 2′-F-α-L-RNA monomer displays many of the same characteristics as the corresponding α-L-RNA and α-L-LNA monomers, but because of its duplex destabilizing effect it cannot be considered a monocyclic version of an α-L-LNA monomer.

Experimental Section

1-(2-*O*-Acetyl-3,5-di-*O*-benzyl-α-L-arabinofuranosyl)thymine (2): Compound **1**[26] (1.85 g, 4.47 mmol) and thymine (1.13 mg, 8.94 mmol) were coevaporated with anhyd. MeCN (2×10 mL) and resuspended in anhyd. MeCN (25 mL) followed by addition of *N*,*O*-bis-(trimethylsilyl)acetamide (BSA, 3.9 mL, 15.6 mmol) while being stirred at room temperature. The resulting suspension was refluxed until it became a clear solution (>45 min) and was then cooled to room temperature. Trimethylsilyl triflate (TMSOTf, 2.0 mL, 11.2 mmol) was added and the mixture was heated to 80 °C for 25 h. The reaction mixture was cooled to room temperature and poured into sat. aq. $NaHCO_3$ (30 mL) and the resulting mixture was extracted with CH_2Cl_2 (4×100 mL). The combined organic phase was dried (Na_2SO_4), filtered, and evaporated to dryness under reduced pressure. The residue was purified by silica gel column chromatography by using as eluent EtOAc (0–100%) in PE to afford compound **2** as a white foam (1.97 mg; 92%). ^{1}H NMR (400 MHz, $CDCl_3$): δ = 8.53 (s, 1H; NH), 7.36–7.05 (m, 11H; Ph and H6), 6.05 (d, J = 2.3 Hz, 1H; H1′), 5.22 (t, J = 1.9 Hz, 1H; H2′), 4.67–4.36 (m, 5H; 2×OCH_2Ph and H4′), 4.02 (t, J = 2.1 Hz, 1H; H3′), 3.51 (dd, J = 10.1, 5.7 Hz, 1H; $H5'_a$), 3.44 (dd, J = 10.1, 6.5 Hz, 1H; $H5'_b$), 1.92 (s, 3H; Me), 1.73 (d, J = 1.2 Hz, 3H; Me); ^{13}C NMR (101 MHz, $CDCl_3$): δ = 168.6, 162.5, 149.2, 136.5, 135.8, 134.9, 127.5, 127.5, 127.2, 126.9, 126.8, 126.8, 109.9 (C5), 88.6 (C1′), 84.1 C4′), 81.2 (C3′), 79.5 (C2′), 72.5 (CH_2), 71.1 (CH_2), 68.1 (C5′), 19.7 (Me), 11.4 (Me); elemental analysis calcd (%) for $C_{26}H_{28}N_2O_7$: C 64.99, H 5.87, N 5.83; found: C 64.79, H 5.80, N 5.70; ESI-HRMS: *m/z* 503.1798 ([*M*+Na]$^+$, $C_{26}H_{28}N_2O_7$·Na calcd 503.1789).

1-(2-*O*-Acetyl-3,5-di-*O*-benzyl-α-L-arabinofuranosyl)-3-(benzyloxymethyl)thymine (3): Compound **2** (1.50 g, 3.12 mmol) was dissolved in anhyd. DMF (30 mL) and the resulting mixture was stirred at 0 °C. 1,8-Diazabicyclo[5.4.0]undec-7-ene (DBU, 467 μL, 3.12 mmol) was added followed by dropwise addition of benzyloxymethyl chloride (BOMCl, 520 μL, 3.74 mmol). The reaction mixture

was stirred for 2 h whereupon sat. aq. $NaHCO_3$ (50 mL) was added. The reaction mixture was stirred for additional 10 min followed by extraction with EtOAc (150 mL). The organic phase was washed with H_2O (5×100 mL). The organic phase was dried (Na_2SO_4), filtered and evaporated to dryness under reduced pressure. The residue was purified by silica gel column chromatography by using as eluent EtOAc (0–50%) in PE to afford compound **3** as a colorless oil (1.78; 94%). ^{1}H NMR (400 MHz, $CDCl_3$): δ = 7.39–7.21 (m, 16H; Ph and H6), 6.13 (d, J = 1.9 Hz, 1H; H1′), 5.46 (q, J = 9.7 Hz, 2H; NCH_2), 5.29 (d, J = 8.7 Hz, 1H; H2′), 4.70–4.48 (m, 7H; H4′ and 3×OCH_2), 4.07 (s, 1H; H3′), 3.58 (dd, J = 10.0, 5.7 Hz, 1H; H5′$_a$), 3.51 (dd, J = 10.0, 6.6 Hz, 1H; H5′$_b$), 1.99 (s, 3H; Me), 1.82 (s, 3H; Me); ^{13}C NMR (101 MHz, $CDCl_3$): δ = 169.6 (C=O), 163.4 (C=O), 151.0 (C=O), 138.0 (Ph), 137.6 (Ph), 136.9 (Ph), 134.6 (C6), 128.5 (Ph), 128.3 (Ph), 128.1 (Ph), 128.0 (Ph), 127.8 (Ph), 127.7 (Ph), 127.6 (Ph), 110.2 (C5), 90.5 (C1′), 85.4 (C4′), 82.3 (C3′), 80.5 (C2′), 73.5(CH_2), 72.1(CH_2), 72.0 (CH_2), 70.5 (CH_2), 69.2 (C5′), 20.7 (Me), 13.2 (Me); elemental analysis calcd (%) for $C_{34}H_{36}N_2O_8 \cdot {}^1/_2\,H_2O$: C 66.98, H 6.12, N 4.59; found: C 66.61, H 5.80, N 4.29; ESI-HRMS: m/z 623.2350 ([M+Na]$^+$, $C_{34}H_{38}N_2O_8$·Na calcd 623.2364).

1-(3,5-Di-*O*-benzyl-α-L-arabinofuranosyl)-3-(benzyloxymethyl)-thymine (4): Compound **3** (1.70 g, 2.83 mmol) was dissolved in CH_2Cl_2 (20 mL) and sat. methanolic ammonia (60 mL) was added and the reaction mixture was stirred at room temperature for 4 h. The solution was evaporated to dryness under reduced pressure. The residue was purified by silica gel column chromatography by using as eluent EtOAc (0–50%) in PE to give compound **4** as a white foam (1.56 g; 99%). ^{1}H NMR (400 MHz, $CDCl_3$): δ = 7.42–7.17 (m, 16H; Ph and H6), 5.94 (d, J = 1.5 Hz, 1H; H1′), 5.49 (q, J = 9.7 Hz, 2H; NCH_2), 4.72–4.48 (m, 7H; H4′ and 3×OCH_2), 4.29 (d, J = 8.6 Hz, 1H; H2′), 4.18 (d, J = 8.6 Hz, 1H; 2′-OH), 4.05–4.02 (m, 1H; H3′), 3.75 (dd, J = 10.6, 2.9 Hz, 1H; H5′$_a$), 3.65 (dd, J = 10.6, 3.3 Hz, 1H; H5′$_b$), 1.82 (s, 1H; Me); ^{13}C NMR (101 MHz, $CDCl_3$): δ = 163.5 (C=O), 151.4 (C=O), 138.0, 136.9, 136.6, 134.3 (C6), 128.7, 128.6, 128.3, 128.3, 128.1, 128.0, 127.7, 127.7, 127.6, 109.4 (C5), 94.6 (C1′), 85.7 (C4′), 84.8 (C3′), 80.4 (C2′), 74.0 (CH_2), 72.3 (CH_2), 72.0 (CH_2), 70.5, 70.3 (C5′), 13.2 (Me); elemental analysis calcd (%) for $C_{32}H_{34}N_2O_7$: C 68.80, H 6.13, N 4.69; found: C 68.50, H 5.76, N 4.69; ESI-HRMS: m/z 581.2279 ([M+Na]$^+$, $C_{32}H_{34}N_2O_7$·Na calcd 581.2259).

1-(2-Deoxy-3,5-di-*O*-benzyl-2-fluoro-α-L-ribofuranosyl)-3-(benzyloxymethyl)thymine (5): Compound **4** (1.50 g, 2.69 mmol) was co-evaporated with anhyd. toluene (2×20 mL) and redissolved in anhyd. toluene (25 mL) and the resulting mixture was stirred at room temperature. Anhyd. pyridine (1.1 mL, 13.5 mmol) and deoxo-fluor (50% in toluene, 3.9 mL, 10.8 mmol) were added and the reaction was stirred for 20 h at room temperature. The reaction mixture was diluted with EtOAc (100 mL) and washed successively with sat. aq. $NaHCO_3$ (50 mL) and brine (50 mL). The organic phase was dried (Na_2SO_4), filtered and evaporated to dryness under reduced pressure. The residue was purified by silica gel column chromatography by using as eluent EtOAc (0–50%) in PE to afford compound **5** as a colorless oil (775 mg; 50%). ^{1}H NMR (400 MHz, $CDCl_3$): δ = 7.39–7.18 (m, 15H; Ph), 7.15 (d, J = 1.2 Hz, 1H; H6), 6.11 (dd, J = 16.2, 1.3 Hz, 1H; H1′), 5.48 (q, J = 9.7 Hz, 2H; NCH_2), 5.17 (dt, J = 49.8, 1.4 Hz, 1H; H2′), 4.71–4.54 (m, 7H; H4′ and 3×OCH_3), 4.26–4.18 (m, 1H; H3′), 3.62 (ddd, J = 10.1, 6.0, 1.8 Hz, 1H; H5′$_a$), 3.54 (ddd, J = 10.1, 6.4, 1.2 Hz, 1H; H5′$_b$), 1.83 (d, J = 1.2 Hz, 3H; Me); ^{13}C NMR (101 MHz, $CDCl_3$): δ = 163.3 (C=O), 150.9 (C=O), 138.0, 137.6, 136.4, 134.6 (C6), 128.6, 128.5, 128.4, 128.3, 128.3, 127.9, 127.8, 127.8, 127.7, 109.8 (C5), 97.7 (d, J = 187.6 Hz, C2′), 91.1 (d, J = 37.1 Hz, C1′), 85.5 (C4′), 81.6 (d, J = 25.5 Hz, C3′), 73.6, 72.3, 72.3, 70.5, 69.2 (d, J = 2.6 Hz, H5′), 13.1 (Me); ^{19}F NMR (376 MHz, $CDCl_3$): δ = −185.5; elemental analysis calcd (%) for $C_{32}H_{33}FN_2O_6 \cdot {}^1/_5$ EtOAc: C 68.13, H 6.03, N 4.84; found: C 67.77, H 5.65, N 4.69; ESI-HRMS: m/z 583.2219 ([M+Na]$^+$, $C_{32}H_{33}FN_2O_6$·Na calcd 583.2215).

1-(2-Deoxy-2-fluoro-α-L-ribofuranosyl)thymine (6): Compound **5** (720 mg, 1.28 mmol) was dissolved in anhyd. CH_2Cl_2 (50 mL) and the solution was stirred and cooled to −78 °C by using dry ice and acetone. Boron trichloride (1.0 M solution in CH_2Cl_2, 10.2 mL, 10.2 mmol) was added dropwise and the reaction mixture was stirred for 30 min at −78 °C. Afterwards, MeOH (25 mL) was added and the resulting mixture was allow to warm to room temperature. The reaction mixture was evaporated to dryness under reduced pressure and the residue was redissolved in H_2O (50 mL) and the resulting mixture was stirred for 22 h at room temperature. The mixture was then evaporated to dryness under reduced pressure and the residue was coevaporated with anhyd. MeCN (3×20 mL). The residue was purified by silica gel column chromatography by using as eluent MeOH (10%) in CH_2Cl_2 to afford nucleoside **6** as a white foam (258 mg; 77%). ^{1}H NMR (400 MHz, CD_3CN): δ = 9.21 (br s, 1H; NH), 7.37 (dd, J = 2.3, 1.1 Hz, 1H; H6), 5.95 (dd, J = 16.7, 2.6 Hz, 1H; H1′), 5.15 (dt, J = 51.4, 2.8 Hz, 1H; H2′), 4.40–4.26 (m, 2H; H3′ and H4′), 3.85 (d, J = 4.1 Hz, 1H; 3′-OH), 3.65–3.54 (m, 2H; H5′), 3.06 (t, J = 5.9 Hz, 1H; 5′-OH), 1.83 (d, J = 1.2 Hz, 3H; Me); ^{13}C NMR (101 MHz, CD_3CN): δ = 164.8 (C=O), 151.6 (C=O), 137.7 (C6), 111.1 (C5), 101.0 (d, J = 184.9 Hz, C2′), 90.8 (d, J = 37.0 Hz, C1′), 88.6 (d, J = 3.8 Hz, C4′), 74.9 (d, J = 24.8 Hz, C3′), 62.1 (d, J = 1.8 Hz, C5′), 12.5 (Me); ^{19}F NMR (376 MHz, CD_3CN): δ = −189.33; elemental analysis calcd (%) for $C_{10}H_{13}FN_2O_5$: C 46.16, H 5.04, N 10.77; found: C 45.78, H 4.95, N 10.50; ESI-HRMS: m/z 283.0700 ([M+Na]$^+$, $C_{10}H_{13}FN_2O_5$·Na calcd 283.0701).

1-(2-Deoxy-5-*O*-(4,4′-dimethoxytrityl)-2-fluoro-α-L-ribofuranosyl)thymine (7): Compound **6** (229 mg, 0.88 mmol) was coevaporated with anhyd. pyridine (2×5 mL) and redissolved in anhyd. pyridine (5 mL). 4,4′-Dimethoxytrityl chloride (DMTrCl, 386 mg, 1.14 mmol) was added and the resulting mixture was stirred for 3 h at room temperature. EtOH (0.5 mL) was added and stirring was continued for additional 10 min followed by evaporation to dryness under reduced pressure. The residue was redissolved in CH_2Cl_2 (100 mL) and washed successively with sat. aq. $NaHCO_3$ (25 mL) and brine (25 mL). The organic phase was dried (Na_2SO_4), filtered and evaporated to dryness under reduced pressure. The residue was purified by silica gel column chromatography by using as eluent EtOAc (50–100%) in PE to afford nucleoside **7** as a white foam (448 mg; 88%). ^{1}H NMR (400 MHz, $CDCl_3$): δ = 9.53 (br s, 1H; NH), 7.49–7.41 (m, 2H), 7.37–7.17 (m, 8H), 6.86–6.78 (m, 4H), 5.80 (d, J = 17.8 Hz, 1H; H1′), 5.32 (d, J = 50.2 Hz, 1H; H2′), 4.53–4.38 (m, 2H; H3′ and H4′), 3.78 (s, 6H; 2×OMe), 3.73 (d, J = 5.7 Hz, 1H; 3′OH), 3.31 (dd, J = 9.0, 6.2 Hz, 1H; H5′$_a$), 3.24 (dd, J = 10.2, 5.3 Hz, 1H; H5′$_b$), 1.89 (d, J = 1.1 Hz, 3H; Me); ^{19}F NMR (376 MHz, $CDCl_3$): δ = −181.4; elemental analysis calcd (%) for $C_{31}H_{31}FN_2O_7 \cdot {}^1/_4$ EtOAc: C 65.74, H 5.69, N 4.79; found: C 65.38, H 5.63, N 4.75; ESI-HRMS: m/z 585.2010 ([M+Na]$^+$, $C_{31}H_{31}FN_2O_7$·Na calcd 585.2008).

1-(3-*O*-(2-Cyanoethoxy(diisopropylamino)phosphino)-2-deoxy-5-*O*-(4,4′-dimethoxytrityl)-2-fluoro-α-L-ribofuranosyl)thymine (8): Compound **7** (104 mg, 0.18 mmol) was coevaporated with 1,2-DCE and redissolved in anhyd. CH_2Cl_2 (5 mL) and the resulting mixture was stirred under argon at room temperature. Diisopropyl ammonium tetrazolide (46 mg, 0.27 mmol) and bis(*N*,*N*-diisopropylamino)-2-cyanoethoxyphosphine (85 μL, 0.27 mmol) were added and stirring was continued for 18 h at room temperature. The resulting mixture was diluted with sat. aq. $NaHCO_3$ (25 mL) and extracted with CH_2Cl_2 (2×50 mL). The combined organic phase was dried

(Na_2SO_4), filtered and evaporated to dryness under reduced pressure. The residue was purified by silica gel column chromatography by using as eluent EtOAc (30–40%) in PE to afford phosphoramidite **8** as a white foam (129 mg; 94%); ^{31}P NMR (162 MHz, $CDCl_3$): $\delta = 152.2$, 151.3; elemental analysis calcd (%) for $C_{40}H_{48}FN_4O_8P \cdot {}^1/_{19}$ EtOAc: C 62.93, H 6.36, N 7.30; found: C 62.93, H 6.43, N 6.91; ESI-HRMS: *m/z* 785.3088 ($[M+Na]^+$, $C_{40}H_{48}FN_4O_8P{\cdot}Na$ calcd 785.3086).

General procedure for synthesis and purification of oligonucleotides: Synthesis of ONs was performed on the 0.2 μmol scale by using an automated DNA synthesizer. Standard cycle procedures were applied for unmodified phosphoramidites by using a solution of 1*H*-tetrazole (0.45 M) as activator. Stepwise coupling yields, as determined by a spectrophotometric $DMTr^+$ assay, were >99% for standard phosphoramidites and >95% (15 min coupling time) for phosphoramidite **8**. Removal of the nucleobase protection groups and cleavage from the solid support was effected by using standard conditions (32% aqueous ammonia for 12 h at 55 °C). Unmodified DNA and RNA strands were obtained from commercial suppliers and, if necessary, further purified as described below. Purification of ONs was performed by DMTr-ON RP-HPLC by using the Waters system 600 equipped with Xterra MS C18 column (5 μm, 150×7.8 mm) and a precolumn Xterra MS C18 column (5 μm, 10×7.8 mm) by using the representative gradient protocol depicted in Table S1 in the Supporting Information. Fractions containing pure ONs were collected and evaporated, followed by detritylation (80% aq. AcOH, 20 min), precipitation (acetone, −18 °C, 12 h) and washing with acetone. The composition of ONs was verified by MALDI-MS analysis (Table S3 in the Supporting Information), whereas the purity (>80%) was verified by ion-exchange HPLC by using a LaChrome L-7000 system (VWR International) equipped with a Dionex DNAPac Pa-100 (250×4.0 mm) by using the representative gradient protocol shown in Table S2 in the Supporting Information.

General procedure for thermal denaturation studies: Concentrations of ONs were calculated by using the following extinction coefficients (OD_{260} [μmol]): DNA: A (15.2), G (12.0), T (8.4), and C (7.1); RNA: A (15.4), G (13.7), U (10.0), and C (9.0). Concentrations of modified ONs were calculated as for unmodified DNA strands. ONs (1.0 μmol of each strand) were thoroughly mixed in a T_m buffer (medium salt buffer: 100 mM NaCl, 0.1 mM EDTA, pH 7.0 adjusted with 10 mM NaH_2PO_4/5 mM Na_2HPO_4; high salt buffer: 700 mM NaCl, 0.1 mM EDTA, pH 7.0 adjusted with 10 mM NaH_2PO_4/5 mM Na_2HPO_4), denatured by being heated to 70 °C and subsequently cooled to the starting temperature of the experiment. Quartz optical cells with a path-length of 1.0 cm were used. Thermal denaturation curves (A_{260} vs. temperature) were obtained on a Perkin–Elmer Lambda 35 UV/Vis spectrometer equipped with a PTP-6 Peltier temperature programmer. Thermal denaturation temperatures (T_m values) were determined as the maximum of the first derivative of the melting curve. A temperature ramp of 1.0 °C was used in all experiments. Reported thermal denaturation temperatures are an average of two measurements within ±1.0 °C.

Protocol for CD measurements: Samples for CD measurements were prepared as described for the thermal denaturation studies, although a concentration of 5.0 μM of each oligonucleotide was used. Quartz optical cells with a path-length of 0.20 cm were used. CD spectra were recorded on Jasco J-815 CD spectrometer equipped with CDF 4265/15 temperature controller. The CD spectra (200–400 nm) were measured at 20 °C as an average of five scans by using a slit of 2.0 nm and a scan speed of 100 nm min^{-1}.

Quantum mechanical calculations: Ab initio quantum mechanical calculations were carried out by using the Gaussian 03 program.[33] To determine the potential energy of pseudorotation, sugar torsion angles ν_2 and ν_4 were calculated by using the theory of Altona and Sundaralingam with a maximal puckering amplitude of 36°.[34] For each point along the pseudorotation pathway, full geometry optimizations (MP2/6-31G) were carried out while maintaining the desired ν_2 and ν_4 angles and constraining the ε torsion angle to a value consistent with duplex geometry. Single point energies were determined by using second-order Møller–Plesset theory (MP2) with the cc-pVTZ basis set.

Molecular dynamics calculations: The unmodified DNA:DNA duplex was constructed with a standard B-type helical geometry and the DNA:RNA duplex was constructed with a standard A-type helical geometry. These duplexes were subsequently modified to the duplexes of interest by using the MacroModel V9.1 suite of programs.[31] Furthermore, the negative charge of the phosphodiester was neutralized with sodium ions, which were placed 3.0 Å from the two none-bridging oxygen atoms. The model structures were energy minimized, followed by 5 ns stochastic dynamics simulations during which 1000 structures were collected (300 K, 2 fs time step, SHAKE constraints on all bonds to hydrogen) and these were subsequently energy minimized. The simulations were carried out by using the AMBER force field[28,29] and the GB/SA solvent model.[30] The collected structures were used to calculate the sugar pucker, *P*, the glycosidic torsion angle and the backbone torsion angles. In all calculations, the first 100 structures generated were discarded, as the respective duplexes were not in equilibrium.

Acknowledgements

We gratefully thank The Danish National Research Foundation for funding.

Keywords: ab initio calculations · conformation analysis · L-nucleosides · L-nucleotides · molecular modeling

[1] N. M. Bell, J. Micklefield, *ChemBioChem* **2009**, *10*, 2691 – 2703.
[2] J. Kurreck, *Eur. J. Biochem.* **2003**, *270*, 1628 – 1644.
[3] J. H. P. Chan, S. H. Lim, W. S. F. Wong, *Clin. Exp. Pharmacol. Physiol.* **2006**, *33*, 533 – 540.
[4] D. R. Yazbeck, K. L. Min, M. J. Damha, *Nucleic Acids Res.* **2002**, *30*, 3015 – 3025.
[5] T. P. Prakash, B. Bhat, *Curr. Top. Med. Chem.* **2007**, *7*, 641 – 649.
[6] J. K. Watts, N. Martín-Pintado, I. Gómez-Pinto, J. Schwartzentruber, G. Portella, M. Orozco, C. González, M. J. Damha, *Nucleic Acids Res.* **2010**, *38*, 2498 – 2511.
[7] H. Ikeda, R. Fernandez, A. Wilk, J. J. Barchi, X. L. Huang, V. E. Marquez, *Nucleic Acids Res.* **1998**, *26*, 2237 – 2244.
[8] B. Reif, V. Wittmann, H. Schwalbe, C. Griesinger, K. Wörner, K. Jahn-Hofmann, J. W. Engels, *Helv. Chim. Acta* **1997**, *80*, 1952 – 1971.
[9] S. Uesugi, H. Miki, M. Ikehara, H. Iwahashi, Y. Kyogoku, *Tetrahedron Lett.* **1979**, *20*, 4073 – 4076.
[10] W. Guschlbauer, K. Jankowski, *Nucleic Acids Res.* **1980**, *8*, 1421 – 1433.
[11] A. M. Kawasaki, M. D. Casper, S. M. Freier, E. A. Lesnik, M. C. Zounes, L. L. Cummins, C. Gonzalez, P. D. Cook, *J. Med. Chem.* **1993**, *36*, 831 – 841.
[12] P. Kois, Z. Tocik, M. Spassova, W. Y. Ren, I. Rosenberg, J. F. Soler, K. A. Watanabe, *Nucleosides Nucleotides* **1993**, *12*, 1093 – 1109.
[13] C. J. Wilds, M. J. Damha, *Nucleic Acids Res.* **2000**, *28*, 3625 – 3635.
[14] J. K. Watts, M. J. Damha, *Can. J. Chem.* **2008**, *86*, 641 – 656.
[15] M. J. Damha, C. J. Wilds, A. Noronha, I. Brukner, G. Borkow, D. Arion, M. A. Parniak, *J. Am. Chem. Soc.* **1998**, *120*, 12976 – 12977.
[16] M. M. Mangos, K. L. Min, E. Viazovkina, A. Galarneau, M. I. Elzagheid, M. A. Parniak, M. J. Damha, *J. Am. Chem. Soc.* **2003**, *125*, 654 – 661.

[17] A. E. Håkansson, A. A. Koshkin, M. D. Sørensen, J. Wengel, *J. Org. Chem.* **2000**, *65*, 5161 – 5166.
[18] A. E. Håkansson, J. Wengel, *Bioorg. Med. Chem. Lett.* **2001**, *11*, 935 – 938.
[19] L. Keinicke, M. D. Sørensen, J. Wengel, *Bioorg. Med. Chem. Lett.* **2002**, *12*, 593 – 596.
[20] G. Gaubert, B. R. Babu, S. Vogel, T. Bryld, B. Vester, J. Wengel, *Tetrahedron* **2006**, *62*, 2278 – 2294.
[21] M. D. Sørensen, L. Kværnø, T. Bryld, A. E. Håkansson, B. Verbeure, G. Gaubert, P. Herdewijn, J. Wengel, *J. Am. Chem. Soc.* **2002**, *124*, 2164 – 2176.
[22] J. Wengel, M. Petersen, K. E. Nielsen, G. A. Jensen, A. E. Håkansson, R. Kumar, M. D. Sørensen, V. K. Rajwanshi, T. Bryld, J. P. Jacobsen, *Nucleosides Nucleotides Nucleic Acids* **2001**, *20*, 389 – 396.
[23] M. Petersen, A. E. Håkansson, J. Wengel, J. P. Jacobsen, *J. Am. Chem. Soc.* **2001**, *123*, 7431 – 7432.
[24] J. T. Nielsen, P. C. Stein, M. Petersen, *Nucleic Acids Res.* **2003**, *31*, 5858 – 5867.
[25] K. M. E. Nielsen, M. Petersen, A. E. Håkansson, J. Wengel, J. P. Jacobsen, *Chem. Eur. J.* **2002**, *8*, 3001 – 3009.
[26] J. Ning, F. Z. Kong, *J. Carbohydr. Chem.* **1997**, *16*, 311 – 325.
[27] A. Rodger, B. Nordén, *Circular Dichroism and Linear Dichroism*, Oxford University Press, Oxford, **1997**.
[28] S. J. Weiner, P. A. Kollman, D. A. Case, U. C. Singh, C. Ghio, G. Alagona, S. Profeta, P. Weiner, *J. Am. Chem. Soc.* **1984**, *106*, 765 – 784.
[29] S. J. Weiner, P. A. Kollman, D. T. Nguyen, D. A. Case, *J. Comput. Chem.* **1986**, *7*, 230 – 252.
[30] W. C. Still, A. Tempczyk, R. C. Hawley, T. Hendrickson, *J. Am. Chem. Soc.* **1990**, *112*, 6127 – 6129.
[31] MacroModel, version 9.1 ed., New York, **2005**.
[32] P. Varnai, D. Djuranovic, R. Lavery, B. Hartmann, *Nucleic Acids Res.* **2002**, *30*, 5398 – 5406.
[33] M. J. Frisch, G. W. Trucks, H. B. Schlegel, G. E. Scuseria, M. A. Robb, J. R. Cheeseman, J. A. Montgomery, Jr., T. Vreven, K. N. Kudin, J. C. Burant, J. M. Millam, S. S. Iyengar, J. Tomasi, V. Barone, B. Mennucci, M. Cossi, G. Scalmani, N. Rega, G. A. Petersson, H. Nakatsuji, et al., Gaussian 03, Revision D.02, Gaussian, Inc., Wallingford, CT, **2004**.
[34] C. Altona, M. Sundaralingam, *J. Am. Chem. Soc.* **1972**, *94*, 8205 – 8212.

Received: March 11, 2011
Published online on July 4, 2011

